scientific reports



OPEN

Chitosan composites with beeswax and olive oil nano-microcapsules physicochemical characterization and antibacterial activity against skin microbiota

Liliana Woszczak¹, Karen Khachatryan¹, Magdalena Krystyjan¹, Anna Lenart-Boroń³, Marcel Krzan⁴, Anna Białecka⁵ & Gohar Khachatryan⁶

Polysaccharide-based composites, such as those containing chitosan, offer significant potential due to their biodegradability, non-toxicity and membrane-forming properties. Chitosan, due to its functional groups, is ideal for nano-/microcapsule formation. Encapsulation protects bioactive components from environ-mental stress, improves physicochemical properties and enhances biological and antimicrobial activity. This research has developed a surfactant-free method to produce beeswax and olive oil nano-/microcapsules stabilized solely within a chitosan matrix without synthetic stabilisers or additional surfactants. The formation of gels and films containing these nano/micro capsules was confirmed by scanning electron microscopy (SEM). Incorporation of the nano/micro capsules into the matrix reduced the mechanical properties compared to the control sample, but significantly improved the hydrophobicity and UV barrier properties. Microbiological tests revealed mild antibacterial properties, highlighting the potential of the composites for applications in cosmetics, such as emulsions and creams, and in food technology, as coatings and packaging materials. The encapsulation process enables the straightforward integration of bioactive ingredients, thus expanding the potential applications.

Keywords Beeswax, Encapsulation, Olive oil, Chitosan

Nanotechnology is a multidisciplinary field with applications in pharmaceutical, medical, cosmetic and food industries¹⁻⁴. In food and biomedical contexts, it enables encapsulation and targeted delivery of bioactive substances^{5,6}. The use of pure bioactive compounds is often limited by low solubility, bioavailability and chemical stability. Encapsulation enhances these properties, providing protection and improving health-promoting effects⁷⁻¹⁰. Micro- and nanoencapsulation techniques are vital in product formulation, and selecting safe, effective encapsulation systems is essential.

This study developed nano/microcapsules using beeswax and olive oil as the core, stabilised and carried by chitosan. Previous works report various combinations of these materials, highlighting their synergistic potential 11-14. Chitosan, a biopolymer valued for antimicrobial and film-forming abilities, has been extensively combined with olive oil to produce protective coatings. For example, Pereda et al. 14 observed reduced moisture and vapour diffusion in chitosan/olive oil films with increasing oil concentration. Similarly, chitosan-beeswax composites have been shown to enhance barrier properties in packaging 11. Blends of beeswax and olive oil have also demonstrated therapeutic efficacy in treating skin disorders such as psoriasis and dermatitis 15. However, the extant literature contains an absence of information regarding composites that contain all three

¹Laboratory of Nanomaterials and Nanotechnology, Faculty of Food Technology, University of Agriculture, Balicka Street 122, 30-149 Krakow, Poland. ²Department of Carbohydrates Technology and Cereal Processing, Faculty of Food Technology, University of Agriculture, Balicka Street 122, 30-149 Krakow, Poland. ³Department of Microbiology and Biomonitoring, Faculty of Agriculture and Economics, University of Agriculture in Krakow, 30-059 Krakow, Poland. ⁴Jerzy Haber Institute of Catalysis and Surface Chemistry, Polish Academy of Sciences, Niezapominajek Street 8, 30-239 Krakow, Poland. ⁵Jan Bober Center for Microbiology and Autovaccines, 31-016 Krakow, Poland. ⁶Food Quality Analysis and Assessment, Faculty of Food Technology, University of Agriculture, Balicka Street 122, 30-149 Krakow, Poland. [∞]email: karen.khachatryan@urk.edu.pl

components. It is hypothesised that the combination of these three ingredients will result in the production of a novel composite with unique properties. It is hypothesised that the resultant composites will demonstrate increased hydrophobicity, thus providing protection against moisture, alongside improved barrier properties against oxygen and water vapour and enhanced flexibility due to the plasticising effect of the wax. These composites have considerable potential for application in biodegradable packaging, where the mixture could enhance the strength and water resistance of chitosan films; in cosmetics for stabilising creams and lotions; and in biomedicine as carriers for hydrophobic drugs with controlled release.

Beeswax has long been utilised across various industries. As early as antiquity, it was used in medicinal ointments. Synthesised by the wax glands of worker honeybees, beeswax is a complex organic compound comprising: (1) fatty acid and alcohol esters (70–80%), notably myricyl palmitate; (2) hydrocarbons (12–16%), such as hentriacontane ($C_{31}H_{64}$); (3) free fatty acids (10–15%), including cerotic acid ($C_{26}H_{52}O_2$) and neocerotic acid; (4) free alcohols (1–2%), such as myricyl alcohol ($C_{30}H_{61}OH$); and (5) minor constituents (<1%), encompassing pigments (e.g., β -carotene), trace vitamin A, and aromatic compounds 16,17 .

Its diverse applications are well documented. In cosmetics, beeswax functions as an emollient and protective agent in products such as creams, lip balms and lotions. In pharmaceutics, it serves as a base in ointments, coatings, and dressings. The food industry uses beeswax as a glazing agent (E901), anti-caking additive, and for creating edible coatings that extend the shelf life and quality of fruits and vegetables¹⁸. It is also employed as a carrier for additives and as a texturiser in chewing gum^{19–24}. In medicine, beeswax is used in microneedle production, drug coatings for localised delivery, and occlusive dressings for treating dermatitis and burns^{22,24–27}.

Olive oil, extracted from the fruit of the olive tree, is a core component of the Mediterranean diet 28,29 . Its principal fatty acids—oleic, linoleic and linolenic—are known for their nutritional benefits and role in supporting skin barrier function. These acids aid in the penetration of active ingredients and serve protective or moisturising functions 30,31 . Beyond fatty acids, olive oil contains phenolic compounds, including α -tocopherol and carotenoids, as well as vitamins E and K, making it a valuable ingredient in cosmetic formulations such as shampoos, creams, soaps and lotions $^{32-34}$.

Chitosan, a biodegradable and biocompatible polysaccharide derived from chitin and primarily composed of glucosamine and N-acetylglucosamine units, has gained significant attention in industrial applications, particularly in food packaging, due to its antimicrobial, antifungal, and film-forming properties³⁵. Chitosan coatings extend shelf life by inhibiting microbial growth and reducing oxidation, offering a sustainable alternative to synthetic plastics^{36–38}. Its films also provide excellent gas barrier properties, well-suited to preserving perishable goods^{39,40}.

Given its skin-protective properties, olive oil may also influence the skin microbiota, the balance of which is closely linked to the proper functioning of skin itself. Rich composition of olive oil's phenolic compounds such as hydroxytyrosol, tyrosol, and oleocanthal exhibits antioxidant and anti-inflammatory properties that may support skin barrier function and help managing skin conditions linked to microbial imbalances⁴¹. However, research examining the interaction between olive oil and skin microbiota is limited. While numerous studies have explored the effects of olive oil on gut microbiota, investigations into its impact on skin microbial communities or its individual components are still scarce, and these that have been conducted, suggest that the effect—if any—is indirect. For this reason olive oil has been used in this study not as an antimicrobial agent or any type of agent that might affect the skin microbiota, but rather with respect to its properties as effective vehicle for active compounds.

The above mentioned balanced skin microbiota is defined as a diverse community of microorganisms comprising bacteria, fungi, viruses, microeukaryotes, and archaea⁴². Most (<90%) of human skin microbiota includes bacteria of four types: Actinobacteria (36-52%), Firmicutes (24-34%), Proteobacteria (11-16%) and Bacteroidetes (6-9%)⁴³. Among these, coagulase-negative Staphylococus epidermidis, anaerobic Cutibacterium acnes (formerly Propionibacterium acnes), Corynebacterium, Micrococcus, Streptococcus and Acinetobacter are the predominant taxa and these are considered commensal and mutualistic inhabitants of healthy human skin⁴⁴. The skin microbiota density ranges between 10²–10⁷ bacterial cells per cm² of the skin⁴⁵. The abundance, composition and diversity of skin microbiota is shaped by a variety of intrinsic factors (such as skin physiology, sebaceous gland activity, immune status, gender, age, genetics, and host health) as well as extrinsic factors (including geographical location, climate, seasonality, personal hygiene, use of cosmetics and medications)⁴². Sebaceous sites (e.g., face, back) tend to harbor more Cutibacterium, while moist areas (e.g., armpits, groin) are enriched in Corynebacterium and Staphylococcus, and dry areas (e.g., forearms, legs) display greater microbial diversity with an abundance of Proteobacteria and Micrococcus⁴⁵. Even though the composition of skin microbiota is generally consistent in healthy humans, perturbations in its structure (often referred to as dysbiosis) have been linked to various dermatological conditions. For instance, disproportionate proliferation of Cutibacterium acnes is associated with acne vulgaris, while reduced microbial diversity and shifts in Staphylococcus aureus abundance are characteristic of atopic dermatitis and psoriasis^{43,46}. Understanding the factors that influence skin microbiota composition is therefore critical for developing microbiome-based strategies for skin health and disease management⁴⁵.

The objective of this study was twofold. Firstly, the aim was to develop a method for the preparation of chitosan composites containing nano/microcapsules of beeswax and olive oil without the use of additional stabilisers and emulsifiers. Secondly, we aimed to examine the physicochemical and antibacterial (i.e. their effect against pathogenic and commensal microbiota of human skin) properties of the resulting materials.

Materials and methods Materials

Chitosan (2000–3500 cps, very high molecular weight, average molecular weight—1,800,000, degree of deacetylation≥90.0%), acetic acid (99%) and glycerine (99.5%) were purchased from Pol-Aura (Pol-Aura,

Morag, Poland). The beeswax (Cera Flava, cosmetic grade) and olive oil (Olea Europaea (olive) oil, cosmetic grade) were procured from Ecoflores (Ecoflores, Nowy Targ, Poland). Mueller–Hinton II Agar (Biomaxima, Lublin, Poland), Columbia Agar+Sheep Blood (COLS+; Oxoid, Great Britain), Columbia Nalidixic Acid agar (CNA; Oxoid, Great Britain), antimicrobial discs: cefoxitin, erythromycin, clindamycin (Oxoid, Great Britain), deionised water, sterile 0.85% saline solution (Biomaxima, Lublin, Poland).

Preparation of nanoemulsion containing beeswax

A total of 80.0 g of beeswax emulsion was prepared by placing 10.0 g of beeswax, 40.0 g of olive oil and 30.0 g of deionised water in a conical flask (volume 100 ml), which was then placed in an ice bath (temperature 2 °C) and sonified (20 kHz, Sonopuls HD 4200, Bandelin, Berlin, Germany) for 25 min to obtain a homogeneous emulsion.

Preparation of control sample

A 2% chitosan gel was prepared according to a method described in the literature. This involved dissolving 10.0 g of chitosan and 5.0 g of glycerin in 485.0 g of 0.5% acetic acid, which was then heated on a magnetic stirrer (Heidolph RZR 2020, Heidolph Instruments GmbH & Co. KG, Schwabach, Deutschland, German) at 70 °C until a homogeneous suspension was obtained. The resulting gel was subjected to ultrasonication (15 min, 20 kHz, Sonopuls HD 4200, Bandelin, Berlin, Germany). The resulting gel was divided into two parts. The first part was used for microbiological testing without further processing. The second part was transferred to a 150 mm diameter Petri dish and dried completely at 37 °C in a forced-air oven (Memmert UN110, Memmert GmbH, Schwabach, Germany) for 24 h. A control film (SIV1) was obtained.

Encapsulation and sequential fabrication of chitosan-beeswax nanoemulsion samples (gels and films)

In order to stabilise the emulsion and obtain spherical structures, the emulsion obtained in point 2.2 was then introduced into the chitosan gel according to the procedure described below.

To 400.0 g of 2% chitosan gel, 4.0 g of previously prepared beeswax emulsion was added. Mixed with a ultrasonic homogeniser (15 min, 20 kHz, Sonopuls HD 4200, Bandelin, Berlin, Germany) until a homogeneous sample was obtained. The resulting gel was divided into two parts. The first part was used for microbiological testing without further processing. The second part was transferred to a 150 mm diameter Petri dish and dried completely at 37 °C in a forced-air oven (Memmert UN110, Memmert GmbH, Schwabach, Germany) for 24 h. A composite film (SIV2) was obtained.

To the remaining 300.0 g of 2% chitosan gel with emulsion, a further 3.0 g of previously prepared beeswax emulsion was added, mixed with a ultrasonic homogeniser (15 min, 20 kHz, Sonopuls HD 4200, Bandelin, Berlin, Germany) until a homogeneous sample was obtained. The resulting gel was divided into two parts. The first part was used for microbiological testing without further processing. The second part was transferred to a 150 mm diameter Petri dish and dried completely at 37 °C in a forced-air oven (Memmert UN110, Memmert GmbH, Schwabach, Germany) for 24 h. A composite film (SIV3) was obtained.

To the remaining 200.0 g of 2% chitosan gel with emulsion, another 2.0 g of beeswax emulsion was added, mixed with a ultrasonic homogeniser (15 min, 20 kHz, Sonopuls HD 4200, Bandelin, Berlin, Germany) until a homogeneous sample was obtained. The resulting gel was divided into two parts. The first part was used for microbiological testing without further processing. The second part was transferred to a 150 mm diameter Petri dish and dried completely at 37 °C in a forced-air oven (Memmert UN110, Memmert GmbH, Schwabach, Germany) for 24 h. A control film (SIV4) was obtained.

Table 1 presents the composition of each component in the samples tested on a dry weight basis.

All tests listed in the following sections, the purpose of which was to determine the physicochemical and structural properties, were carried out on dried samples – films. It should be noted that the analysis was conducted exclusively on diluted gels, with the focus being on Particle Size and Zeta Potential Analysis. Furthermore, microbiological tests were performed on both gels and films (composites).

Figure 1 presents a schematic of the nanocapsule synthesis. A chitosan shell (derived from 2% gel) encapsulates a nanoemulsified hydrophobic core comprising beeswax and olive oil.

UV-Vis spectroscopy

Spectra were recorded using a scanning spectrophotometer (SHIMADZU TCC-260, Kyoto, Japan) in the 200–700 nm range. The resulting composite films ($8 \times 40 \text{ mm}^2 \text{ strips}$) were measured in a quartz cuvette (10 ml, 10 mm thick quartz cells). An empty cuvette was used as a reference sample.

Sample	Chitosan [g]	Beeswax [g]	Olive Oil [g]	Glycerine [g]
SIV1	2.0	-	-	1.0
SIV2	2.0	0.5	2.0	1.0
SIV3	2.0	1.0	4.0	1.0
SIV4	2.0	1.5	6.0	1.0

Table 1. Ingredient content of the samples, expressed on a dry weight basis.

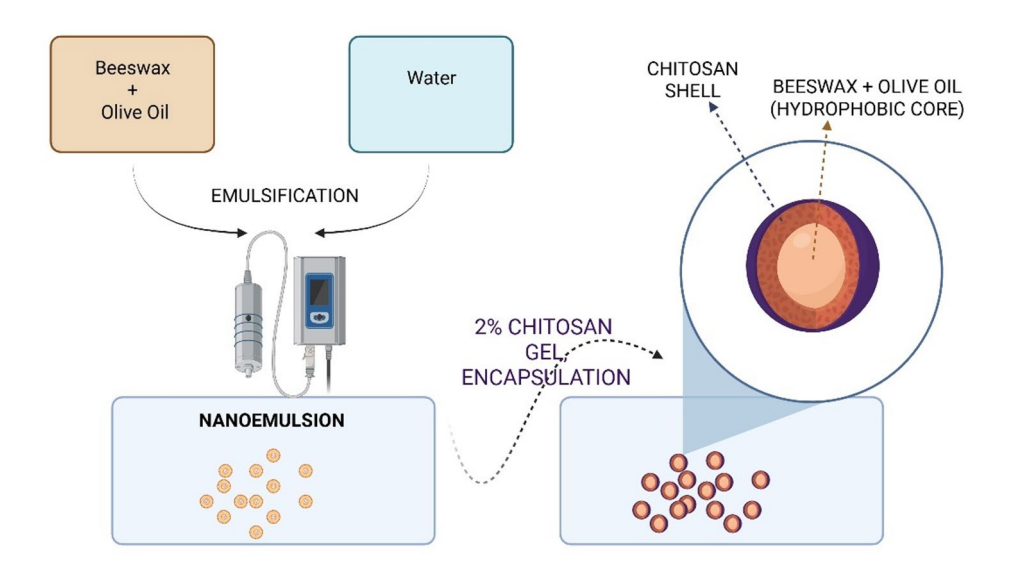


Fig. 1. Schematic diagram of nanoemulsion formation (beeswax/olive oil) and encapsulation within chitosan gel to form core-shell nanocapsules.

Fourier transform infrared attenuated total reflection (FTIR-ATR) spectroscopy

The FTIR-ATR spectra of the beewax, olive oil, chitosan and composite films were analysed with a MATTSON 3000 spectrophotometer (Madison, WI, USA). Spectra were recorded at a resolution of 4 cm⁻¹ and 64 scans in the range of 4000 to 700 cm⁻¹. The spectrophotometer was equipped with a 30SPEC 30-degree reflectance adapter (MIRacle ATR, PIKE Technologies Inc., Madison, WI, USA), which was used to facilitate the measurement of reflectance.

Colour measurements

The colour measurement of the film surface was conducted utilising the Konica MINOLTA CM-3500d equipment (Konica Minolta Inc., Tokyo, Japan), with a 30 mm diameter measuring window, employing a D65/10° observer reference illumination. The results were expressed in accordance with the CIELab system. The following parameters were thus determined: L*, a* and b*. The lightness parameter L* assumes a value of 0 for black and 100 for white. The parameter a* indicates the proportion of green (a*<0) or red (a*>0), while the parameter b* indicates the proportion of blue (b*<0) or yellow (b*>0) 34 . All measurements were made against a standard white background. The final result was obtained by averaging the values from five repetitions. In addition, the following C* and h* parameters were calculated. Chroma (C*) or saturation describes the degree of difference in hue compared to a grey colour with the same luminosity. The higher the saturation values, the higher the colour intensity of the samples perceived by humans.

Hue angle (h*) is the degree value that corresponds to the three-dimensional colour diagram (i.e., 0 for red, 90 for yellow, 180 for green, and 270 for blue) as seen by the human eye⁴⁷. On the basis of the data obtained, the following parameters of colour differences (ΔL^* , Δa^* and Δb^*) as well as total colour difference (ΔEab^*) that is based on L^* , a^* , b^* were calculated. The total colour difference ($\Delta E_{ab}^{}$) was represented by the difference in colour between the films and the standard (sample SIV1).

Opacity measurements

The degree of film opacity was determined spectrophotometrically at 600 nm using a Helios-Gamma 100–240 UV/V spectrophotometer⁷. The rectangular film samples were positioned directly within the test cell of the spectrophotometer, with an empty test cell serving as a reference. The opacity of the film (O) was calculated according to the following equation:

$$O = A_{600}/x \tag{1}$$

where A_{600} is the absorbance at 600 nm, and x is the film thickness [mm]. The analyses were conducted in five replicates.

Scanning electron microscopy (SEM)

The dimensions and morphology of the manufactured nanocapsules were examined using a JEOL 7550 scanning electron microscope (Akishima, Tokyo, Japan). Prior to undertaking the measurements, the samples were subjected to a coating process (K575X Turbo Sputter Coater) involving the deposition of 20 nm of chromium (Cr), with the objective of enhancing the conductivity of the samples.

Particle size and zeta potential analysis

The resulting SIV1-SIV4 gels were diluted with water and assessed for particle size dispersion and zeta potential using a Zetasizer Nano Series ZS (Malvern, UK). The Zetasizer is capable of analysing particles with a size range of approximately 3 nm to 10,000 nm, with an instrument error of 2 nm. The average zeta potential measurement error (standard deviation) was a maximum of 5 mV. All experiments were conducted at room temperature (22 °C). Measurements were repeated three times and the average value from all experiments was calculated.

Mechanical properties of composite films

Prior to analysis, dry composite films were conditioned for 48 h in desiccators maintained at 25 °C and 52% relative humidity (RH) using saturated magnesium-6-water nitrate solutions.

The thickness of the composite films was determined using a micrometer (catalog no. A Sylvac SA (Crissier, Switzerland) digital micrometer with a resolution of 0.001 mm was used. The average thickness of the sample was determined by taking five measurements at different locations on the sample and calculating the mean value⁴⁸.

The samples for textural analysis and the test were performed in accordance with the standards set forth in ISO $527-1:2019^{49}$. The mechanical properties of the film were evaluated using a TA-XT plus texture analyser (Stable Micro Systems, Haslemere, UK). Film strips $(35\times 6~\text{mm}^2)$ were prepared and subsequently positioned within the holders of the measuring instrument. The initial distance between the holders was set at 20 mm, with a tensile rate of 2 mm per minute. Tensile strength (TS) was calculated by dividing the maximum force at break of the film by the cross-sectional area of the film. The elongation percentage (EAB) was calculated by dividing the elongation at break by the initial distance between the grips and multiplying the result by 100, in accordance with the methodology described in reference⁵⁰. The final result was obtained by calculating the mean of the 10 repetitions.

Contact angles and surface free energy of composite films

Contact angles and surface free energy were determined utilising a Kruss Drop Shape DSA100M analyser in conjunction with a digital camera and an environmental chamber. The surface free energy was analysed using the Owens–Wendt method, as previously described in the literature 51,52 , with some modifications. In this methodology, two liquids were employed: one polar (water) and one non-polar (diodomethane). This approach is widely regarded as the most effective for evaluating polymeric substances. The temperature of the test chamber was maintained using a thermostatic water bath, ensuring a constant temperature (22 ± 0.3 °C) and humidity of 50%. At least five consecutive measurements were conducted for each sample.

Characteristics of microorganisms used in the tests

The bacterial strains were obtained from the collection of the Department of Microbiology and Biomonitoring at the University of Agriculture in Kraków. The bacterial strains were subjected to antimicrobial susceptibility tests, following the methodology provided by the European Committee on Antimicrobial Susceptibility Testing⁵³. The susceptibility to three reference antibiotics was examined, i.e. cefoxitin (FOX 30 μg)—a cephalosporin, erythromycin (E 15 μg)—a macrolide and clindamycin (DA 2 μg)—a lincosamid. The bacterial cultures were suspended in sterile 0.85% NaCl solution to obtain 0.5 MacFarland suspensions, which were then streaked onto Mueller-Hinton II agar (Biomaxima, Lublin, Poland). The antimicrobial discs were placed on the surface of agar and the cultures were grown at 36 ± 1 °C for 18-24 h. After that time, growth inhibition zones were measured and the strains were assessed susceptible or resistant based on the breakpoint tables by EUCAST⁵³. The methicillin resistance of staphylococci was assessed based on their reaction (susceptible vs. resistant) to the disc containing cefoxitin (FOX 30 µg). The mechanism of resistance to macrolides, lincosamids and streptogramins b (MLSb) was examined following the methodology described by⁵⁴. The erythromycin-clindamycin disc pairs were placed by hand at a distance of 15-26 mm from the disc edges. After incubation at 35±1 °C for 18-24 h, the results were examined by assessing whether the strains were resistant or susceptible to erythromycin and clindamycin and whether the growth inhibition zone around the DA 2 µg disc was flattened from the side of E 15 µg disc, indicating an inducible type of resistance.

Antibacterial activity of bioactive compounds

The antibacterial activity of preparations containing beeswax capsules and olive oil was investigated using liquid emulsions at four concentrations (SIV1-SIV4) using 11 bacterial strains to determine the minimum inhibitory concentration (MIC). The liquid emulsions were subjected to a 30-min ultraviolet (UV) light sterilisation process.

Bacterial cultures were transferred to sterile 0.85% saline solutions in order to obtain MacFarland 0.5 suspensions, which were then striked onto Mueller–Hinton agar (Argenta, Poland). The antimicrobial effect of the emulsions was assessed through the agar well diffusion method, which entailed the creation of a well in the agar and the subsequent pouring of 100 μ L of the suspensions into the wells. The examined preparations included: SIV1-SIV4 composite emulsions as well as sole olive oil, chitosan and beeswax as individual controls. The cultures were incubated at 36 ± 1 °C for a period of 24 h. Following the incubation period, the results were evaluated by measuring the diameter of the growth inhibition zone surrounding the wells. The growth inhibition zones were expressed in mm. The growth inhibition zones were not produced by smaller concentrations of the examined composites, the SIII inhibited the growth of three strains, while the SIV inhibited the growth of five bacterial strains. This was the highest obtained concentration examined in this study and inhibited the growth of the highest number of bacterial strains, hence this was assessed as the most effective concentration in antibacterial activity (Table S1). A second round of testing was conducted using the sample that exhibited the strongest antibacterial activity and the respective controls.

A total of 36 bacterial isolates were used in the second round of experiment, comprising 22 strains derived from skin lesions, 13 strains of human skin microbiota, isolated from hands and face (cheeks and under eye region) and one *S. aureus* type strain (ATCC 25923).

Statistical analysis

The statistical analysis was conducted using the Statistica software, version 13.3 (StatSoft, Tulsa, OK, USA). The one-way analysis of variance (ANOVA) and Fisher's exact test were performed at the 0.05 level of significance.

Results and discussion UV–Vis spectroscopy

UV–Vis spectroscopy serves as a valuable tool for characterising materials across diverse scales, ranging from nanoparticles to bulk solids. This technique can provide insights into a material's composition, structure, and interactions with light⁵⁵.

Figure 2 illustrates the ultraviolet-visible spectra of the manufactured composite films. A diverse array of bands was discerned, spanning a range of 250 to 375 nm for the control sample (SIV1) and a broader range of 250 to 500 nm for the samples containing beeswax (SIV2, SIV3 and SIV4). The spectra of beeswax exhibit absorption peaks within the ultraviolet (UV) range of 200 to 400 nm, with a maximum absorption observed at 290 nm⁵⁶. In olive oil, the characteristic absorbance between 300 and 500 nm has been linked to different classes of phenolic compounds⁵⁷. The primary visible bands are situated between 200 and 400 nm, which is within the near ultraviolet region. It can be concluded that these bands originate from the excitation of $n \to \pi^*$ (C=C) antibinding electrons and from transitions of binding orbitals to $\pi \to \pi^*$ (C = O) non-binding orbitals⁵⁸. The shape and interactions of a molecule can influence absorption wavelengths, particularly in $\pi \to \pi^*$ transitions. Intermolecular interactions may lead to alterations in the absorption spectrum. In samples containing nanocapsules, an increase in absorbance and a characteristic peak at 265-270 nm were observed. This same effect was noted in our previous studies^{7,10}. UV-Vis absorption features in a material can have significant implications for its functionality, particularly in fields such as optics, electronics, and materials science. The presence and characteristics of these absorptions may determine how a material interacts with light, influencing its capacity to transmit, reflect, or absorb electromagnetic radiation. Such interactions may also impact the material's electronic and chemical properties. Additionally, UV-Vis absorptions can offer information about the material's chemical structure and composition. Specific wavelengths at which absorption occurs may correspond to characteristic functional groups or molecules within the material. The samples containing beeswax nanostructures exhibited a higher level of absorbance than the control sample. Furthermore, the absorption capacity is directly proportional to the concentration of nanoparticles in the matrix. This suggests that the incorporation of nanostructures enhanced the ultraviolet barrier properties of the resulting films, which is in accordance with previous studies^{7,34,59,60}.

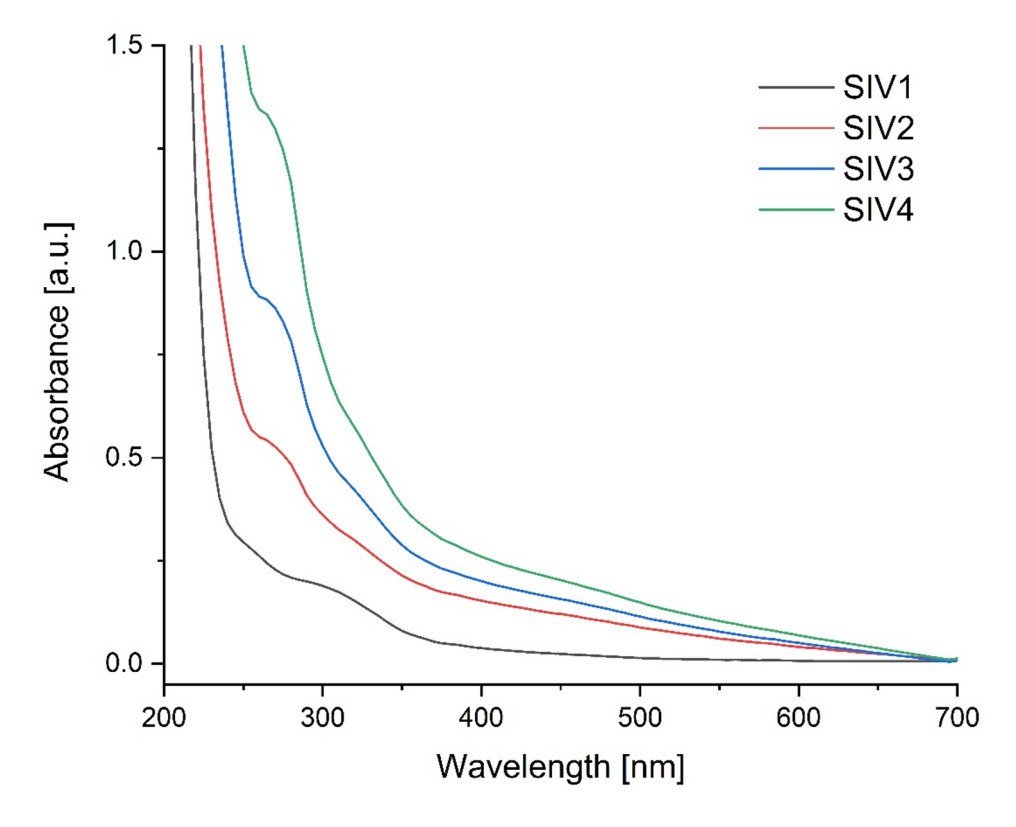


Fig. 2. UV-VIS spectra of obtained composite films.

Fourier transform infrared attenuated total reflection (FTIR-ATR) spectroscopy

Figure 3 depicts a comparative analysis of FTIR-ATR spectra within the spectral range of 700–4000 cm⁻¹ of olive oil and beeswax with those of SIV1, SIV2, SIV3 and SIV4 composite films. The spectrum of beeswax exhibited discernible infrared absorption peaks at 2954, 2915, 2849, 1744, 1460, 1373, and 1157 cm⁻¹. The peaks at 2915 and 2849 cm⁻¹ indicate the presence of fatty acid chains, which can be attributed to stretching vibrations of C–H groups. The peak at 1744 cm⁻¹ is due to stretching vibrations of ester carbonyls. The peaks at 2954 and 1460 cm⁻¹ are attributed to the vibrations of hydrocarbons, while the peaks at 1373 and 1220–1150 cm⁻¹ are indicative of amide groups¹². The asymmetric and symmetric stretching vibrations of the –CH₂ and CH₃ groups, occurring at wave numbers 2915 cm⁻¹ and 2849 cm⁻¹, are also present in the spectrum of olive oil^{8,61}.

wave numbers 2915 cm⁻¹ and 2849 cm⁻¹, are also present in the spectrum of olive oil^{8,61}.

The spectrum of the control sample (SIV1) comprises characteristic bands for chitosan composite films, as previously documented in the literature^{9,10,62,63}. The broad band observed at 3257 cm⁻¹ is associated with the stretching vibrations of the –OH and –NH₂ groups. Furthermore, the presence of carbonyl groups (C=O)^{9,64} is indicated by the appearance of bands at 1744 cm⁻¹. The peak at 1028 cm⁻¹ is attributed to the stretching of C–O and vibrations of O–H in chitosan⁶⁵. The notable disparity between the spectrum of the control sample and those containing beeswax capsules can be attributed to the presence of olive oil and beeswax. In the samples containing beeswax capsules, intense bands are observed at wavelengths of 2915 and 2849 cm⁻¹, resulting from asymmetric and symmetric vibrations of saturated hydrocarbons, respectively.

The absorption bands appear to be similar across all films, indicating that the encapsulation process did not affect the chitosan structure. In the spectra obtained for films containing beeswax and oil, bands corresponding to the encapsulated components are observed. The decrease in absorbance intensity of the band at 3257 cm⁻¹ in samples containing capsules suggests the involvement of –OH and –NH₂ groups in the stabilisation of the nanoemulsion. The reduction in absorbance intensity and slight shifts in the bands for samples containing capsules with wax and oil may be attributed to variations in water content^{9,66}. The addition of oil and wax increased the hydrophobicity of the sample.

Colour measurements and opacity

Table 2 presents a series of parameters that characterise the colour of the surface of the resulting films. Colour is defined by three parameters: tone (hue), saturation (chroma) and lightness (L*). The L* parameter is used to describe the brightness (luminance) of a given colour. The range is from 0 to 100, with 100 indicating the brightest colour¹⁰. Lightness is related to the amount of light reflected or transmitted through an object. Colour is therefore perceived as light or dark. The analysed biocomposites exhibited high luminance, from 95 to 97 (Tab. 2), which was was comparable with chitosan film developed by Velickova et al.⁶⁷. Nevertheless, the incorporation of beeswax and olive oil to chitosan matrix resulted in a slight reduction (from 1.3 to 3.2%) in this parameter. Chitosan gel, like its films, has a high transparency. Beeswax, on the other hand, can vary in colour. Fresh wax is colourless or white, while darkening and browning is caused by admixtures of bee putty or pollen, among other things⁶⁸. The a* coordinate represents the proportion of green (negative values) or red (positive values).

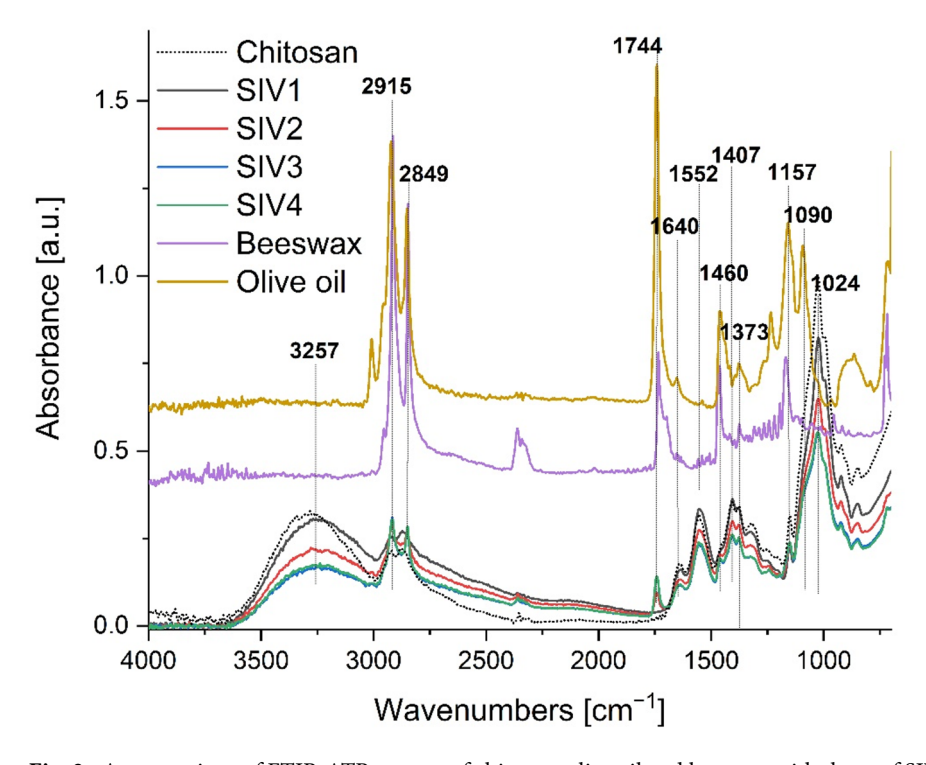


Fig. 3. A comparison of FTIR-ATR spectra of chitosan, olive oil and beeswax with those of SIV1, SIV2, SIV3 and SIV4 composites.

Sample	L*(D65)	a*(D65)	b*(D65)	C*	h*	ΔEab*	O(-)
SIV1	98.32 ± 0.05^{d}	-0.01 ± 0.01^{a}	6.45 ± 0.06^{d}	6.53 ± 0.07^{d}	178.58 ± 0.00^{a}	-	0.40 ± 0.05^{d}
SIV2	97.04 ± 0.08^{b}	-1.61 ± 0.03^{b}	$12.82 \pm 0.40^{\rm c}$	$12.92 \pm 0.40^{\rm c}$	178.55 ± 0.00^{b}	6.53 ± 0.41°	4.66 ± 0.15°
SIV3	95.82 ± 0.22 ^c	-1.90 ± 0.03^{d}	17.47 ± 0.74^{b}	17.57 ± 0.74^{b}	178.54 ± 0.00°	11.34 ± 0.77 ^b	5.71 ± 0.14^{a}
SIV4	95.21 ± 0.10^{a}	-1.84 ± 0.01^{c}	18.76 ± 0.40^{a}	18.85 ± 0.39^a	178.53 ± 0.00^{d}	12.72 ± 0.41 ^a	$5.41 \pm 0.07^{\mathrm{b}}$

Table 2. Colour of the biocomposites and their opacity. * L*, lightness (0 = black, 100 = white); a*, green/red coordinate; b*, blue/yellow coordinate; C*, chroma; h*, hue angle; ΔEab^* , total colour difference; O*, opacity. The values are expressed as the mean ± standard deviation. The presence of the same superscript letter (a, b, c or d) in each column indicates that there is no statistically significant difference between the values in question (p < 0.05).

Conversely, the b^* coordinate is associated with positive values for yellowish colours and negative values for bluish colours³⁴. All samples exhibited a predominant green and yellow share of colour. A notable distinction was evident in the b^* parameter, where an increase in the concentration of wax in the film resulted in a noticeable enhancement of the yellow colour. It is worth noting that the colour of the samples was more than twice as saturated as that of the control sample (SIV1). The higher the concentration of beeswax emulsion in the composite, the higher the saturation (C^*) of colour. Tone (h^*) is the chromatic characteristic of a colour and determines the type of colour, i.e. whether it is red, green, yellow, etc. This parameters matched with very light yellow colour.

Based on measurements of chromatic values and brightness, the total colour difference (ΔE_{ab}^*) of the biocomposites relative to the standard, which was sample SIV1 (chitosan biocomposite), was also calculated. The obtained data indicate that the differences in perceived colour between the samples (SIV2, SIV3 and SIV4) and the control is clear from values of 6.53 to 12.72. A value in the range $3.5 < \Delta E < 5$ is defined as a clearly noticeable colour difference, while above 5 the observer gets the impression of two different colours^{69–71}.

The opacity of the film was found to increase in proportion to the quantity of wax present. The observed alterations are attributable to the pigmentation of the wax, which is more pronounced than that of the chitosan gel.

Scanning electron microscopy (SEM)

Figures 4A and B illustrate the surfaces of the control sample (SIV1) and the sample containing beeswax capsules (SIV2), respectively, as observed under an electron microscope at a magnification of 2500 times. The surface of the control sample is observed to be smooth, while in the beeswax sample, evenly distributed spherical nanostructures are seen to range in size from a 1000 to 3000 nm. It is noteworthy that the capsules exhibit deformation and/or opening under measurement conditions, namely high vacuum and electron bombardment. The following images illustrate the samples at magnifications of 10,000 and 25,500 times, respectively, for SIV2 (Fig. 4C and D), SIV3 (Fig. 4E and F) and SIV4 (Fig. 4G and H). The presence of spherical structures, comprising a core and a shell, is observed in all samples. The cross-section of the sample also expresses visible spherical structures distributed evenly in the material (Fig. 4I). A similar result was observed for curcumin nanocapsules in a chitosan-alginate matrix⁷. Sample SIV4 (Fig. 4G and H) demonstrates reduced stability under measurement conditions. Complete failure of the capsule and the flow of contents were observed. This is likely due to the high concentration of wax and oil. Similar results were obtained in a paper on propolis encapsulation in hyaluronic acid⁷². The comprehensive analysis confirms the efficacy of the nanoemulsion encapsulation method employing chitosan as both a stabilising shell and a functional matrix. The results align with prior studies in which authors utilised diverse polysaccharide combinations (e.g., alginate, starch, chitosan) to enhance colloidal stability^{7,8,10}. It was demonstrated that chitosan, as a stabilising encapsulant, exhibits superior efficiency compared to sodium alginate, particularly in terms of encapsulation yield8.

At the molecular level, interactions between beeswax and chitosan can occur through several mechanisms that affect the physicochemical and functional properties of the resulting complexes or composites. Beeswax is a mixture of hydrophobic compounds (mainly fatty acid esters and hydrocarbons), and is soluble in oils. Chitosan, conversely, is hydrophilic due to the presence of amino $(-NH_2)$ and hydroxyl (-OH) groups, and undergoes protonation (the transition from $-NH_2$ to $-NH_3^+$) in an acidic environment, which gives it a positive charge. Following sonication, the wax molecules, dissolved in the oil, form an emulsion. Subsequently, a layer of chitosan is formed around the nanoemulsion droplets, thereby stabilising the wax/oil emulsions and forming capsules with a hydrophobic core (wax/oil) and a polymer coating (chitosan).Results from electron microscopy and FTIR-ATR studies confirm the proposed nanocapsule structure (Fig. 1): a hydrophobic core (beeswax and olive oil) stabilised by hydrophobic interactions, encapsulated within a chitosan coating that maintains spherical integrity via hydrogen bonding. This is corroborated by FTIR-ATR spectra, which reveal molecular interactions between components through peak shifts and intensity changes—notably, reduced absorption of $-OH/-NH_2$ groups at 3257 cm⁻¹ and altered bands at 2915 cm⁻¹ (C–H asym. stretch), 2849 cm⁻¹ (C–H sym. stretch), and 1744 cm⁻¹ (C=O ester stretch).

Particle size and zeta potential analysis

The zeta potential (ζ) is employed as a means of ascertaining the stability of the resulting nanoparticles. As the absolute value of the zeta potential increases, the dispersion properties of colloidal particles are enhanced, while simultaneously, electrostatic repulsion forces are intensified. As the zeta potential approaches zero, the

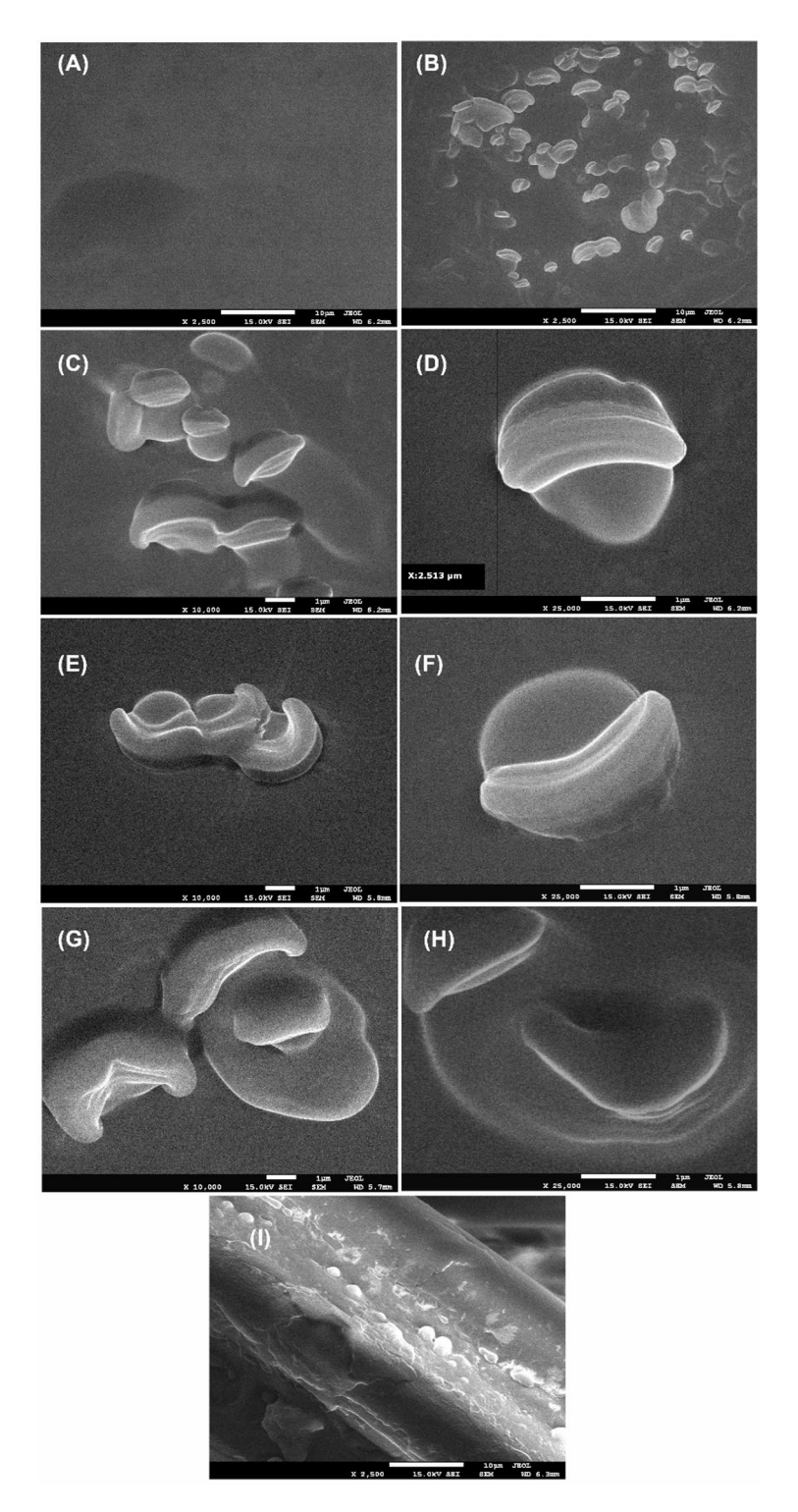


Fig. 4. SEM analysis of control (SIV1, **A**), beeswax capsule modified samples (SIV2, **B**–**D**; SIV3, **E**, **F**; SIV4, **G**, **H**) and cross-section for sample SIV2 (I).

particles become increasingly unstable, leading to a greater propensity for aggregation. It is hypothesised that a result above \pm 30 mV indicates that the test sample is stable ⁷³. The measurement results for individual samples containing beeswax nanocapsules and olive oil were 80 mV, 90 mV, 85 mV and 95 mV for samples SIV1, SIV2, SIV3 and SIV4, respectively. A comparable potential value is observed for chitosan dissolved in acetic acid⁷⁴. The measurement graphs are presented in the supplementary materials (Fig. S1). The zeta potential values for all samples are high, indicating that the system is stable. The generation of nanocapsules in the chitosan matrix resulted in a slight increase in zeta potential values compared to the control sample. This is likely due to the

involvement of chitosan chains in stabilising the surface of the nanoemulsion. In order to ascertain the size and distribution of particles present in the gel, dynamic light scattering (DLS) measurements were performed on the resulting gels (Fig. S2). As illustrated in Figure S2, the distribution is depicted in the left column according to particle number and in the right column according to intensity. The observed discrepancies between the number-based size distribution and the intensity-based distribution are attributable to the polydispersity of the sample and the physical basis of DLS detection. The particle size of the control sample (SIV1) was determined to be 10 nm. The application of an ultrasonic homogeniser in an acetic acid medium resulted in the dispersion of chitosan chains, leading to the formation of nanometric structures. Upon the addition of the initial portion of the beeswax/oil nanoemulsion (sample SIV2), two fractions were observed, with a diameter of 10 nm and 100 nm, respectively. The fraction of 10 nm in diameter was predominant, indicating the formation of nanocapsules with a diameter of 100 nm within the chitosan gel. Upon the addition of a further portion of the nanoemulsion (SIV3), the proportion of particles measuring 100 nm in diameter increased, and these smaller particles were no longer observed. Additionally, a minor population of particles with a diameter of 400 nm was discerned. In sample SIV4, where the largest portion of nanoemulsion was added, particles of 100 nm in size also predominated, but the formation of aggregates of 3000 nm in size was observed. The control sample SIV1 exhibits the lowest polydispersity index (PDI) of 0.28, indicating the most homogeneous particle size distribution. In contrast, samples SIV3 (0.45), SIV2 (0.46), and SIV4 (0.47) display progressively higher PDI values, reflecting increased polydispersity. This trend is likely attributable to the presence of aggregates in these samples. The particle size, as determined by scanning electron microscopy, was found to be within the range of 500 to 1500 nm, while the average particle size, as determined by DLS, was observed to be significantly smaller. This discrepancy may be attributed to the partial aggregation of the particles during the drying process and the deformation of the nanocapsules under the electron beam and vacuum conditions employed for SEM measurements.

Mechanical properties of composite films

Table 3 illustrates the thickness of the films and their corresponding mechanical properties. As can be seen from the data presented, the values of the mechanical parameters of the composite films showed considerable variability. As the amount of beeswax contained in the film increased, so did its thickness. An increase in thickness compared to the control sample (SIV1) by 36-76% was recorded. However, this increase in thickness was accompanied by a 24-62% decrease in film strength. Little variation was observed in the elongation at break parameter. As indicated by the extant literature, the tensile strength (TS) of chitosan composite films is comparable to that of commercial synthetic films, such as HDPE (22-23 MPa) and LDPE (19-44 MPa)⁷⁵. The obtained composites demonstrated greater strength than potato starch-chitosan films with incorporated quantum dots of zinc sulfide and cadmium sulfide (4.6–5.7 MPa)⁷⁶, as well as the kudzu starch-chitosan solution with dissolved chitosan in malic acid (10.13 MPa)⁷⁷. Conversely, the composites produced in this study exhibited a lower tensile strength when compared to cellulose-chitosan composites (> 50 MPa)⁷⁸. Krystyan et al. ³⁴ observed that the thickness of starch/chitosan composites incorporating carbon quantum dots (CQDs) does not always correlate with their breaking strength. In the authors' study, the thin composites demonstrated a 2.5-fold increase in resistance to fracture compared to their thicker counterparts. It has been hypothesised that significantly more robust intermolecular forces are present in thin composites. This is believed to be the reason for their enhanced resistance to breakage. It is also noteworthy that the incorporation of hydrophobic substances into the composition of composites can result in a reduction in breaking strength. However, this is counterbalanced by a concomitant enhancement in the elasticity of the material. The extensibility of the tested composites was comparable to starch/chitosan polymer composites modified by graphene oxide (59.23-66.52%)³⁴, which may be due to the presence of both glycerol and olive oil in the formulation. However, it has been confirmed that while plasticisers have a positive effect on the strength and tensile properties of films by reducing intermolecular friction between the polymer chains⁷⁹, excessive amounts can have the opposite effect⁸⁰. As the concentration of glycerol increases, it has been observed to migrate to the surface of the composite, resulting in a sticky texture⁸¹.

In light of the findings, it is imperative that subsequent utilisation of the composites incorporates a consideration of their modest breaking strength, whilst acknowledging their commendable elongation properties. In scenarios where these parameters may be of paramount importance, it has been demonstrated that the SIV1 composite exhibits the optimal mechanical characteristics among the materials that have been examined.

Contact angles and surface free energy of composite films

The additional hydrophobicity measurements and surface free energy (SFE) evaluations were performed for studied samples. These analysis are pivotal in the evaluation of solid biopolymers, especially in biomedical and

Samp	ole	Thickness* (mm)	TS* (MPa)	EAB* (%)
SIV1		0.116 ± 0.007 ^c	25.71 ± 1.97^{a}	63.83 ± 2.96^{ab}
SIV2		0.158 ± 0.005^{b}	19.36 ± 4.94 ^b	64.51 ± 3.49 ^a
SIV3		0.205 ± 0.011^a	12.14 ± 1.97°	66.21 ± 3.18 ^a
SIV4		0.215 ± 0.021^a	9.72 ± 1.17^{d}	60.13 ± 3.60 ^b

Table 3. Mechanical properties of the obtained films. * TS*, tensile strength (MPa); EAB*, elongation at break (%). The values are expressed as the mean \pm standard deviation. The presence of the same superscript letter (a, b or c) in each column indicates that there is no statistically significant difference between the values in question (p < 0.05).

food production fields^{7,9}. By determining the hydrophilicity and SFE assessments enable us to tailor the material properties for enhanced biocompatibility and performance of potential interactions with biological fluids.

The matrix (control sample—SIV1) of chitosan gel is characterized by high hydrophobicity, which is mainly responsible for dispersive interactions, with a small contribution of polar interactions (Table 4). The addition of beeswax to the chitosan gel matrix increases the value of surface free energy by way of a marked increase in surface dispersive interactions, while polar interactions virtually disappear. The impact of augmented dispersion interactions is already discernible in the sample exhibiting the lowest beeswax content (SIV2). Further increases in concentration result in minimal changes, amounting to a few units of surface free energy.

Antibacterial activity

Skin swabs allowed to gather a total of 35 Gram-positive cocci, mostly belonging to the genus *Staphylococcus*. Detailed characteristics of the strains, including their origin, growth inhibition caused by the reference antibiotics, which are cefoxitin (FOX 30 μ g), erythromycin (E 15 μ g) and clindamycin (DA 2 μ g), type of resistance (methicillin resistance, MLSb type of resistance) and reaction to emulsions containing beeswax biocomposites is provided in Table S1.

The bacterial strains isolated from skin lesions were identified mostly as *Staphylococcus* spp., including the following species: *S. aureus*, *S. warneri*, *S. haemolyticus*, *S. simulans*, *S. epidermidis*, *S. borealis*, *S. lugdunensis* and *S. schleiferi*. They showed a variety of resistance mechanisms. The highest share of resistance was observed in the case of erythromycin (47.6%), followed by clindamycin (38.1%) and cefoxitin, which determined the methicillin resistance of strains (28.6%). As many as 66.7% of lesions-derived strains showed some type of MLS resistance. On the other hand, *Staphylococcus* spp. isolated from healthy human skin, i.e. from hands and under eye region, were all susceptible to erythromycin, one strain (7.7%) was resistant to cefoxitin and two strains (15.4%) were resistant to clindamycin.

Antibacterial activity of the prepared biocomposites was examined in two stages. First, all four (SIV1-SIV4) concentrations were applied along with individual reagents (i.e. chitosan, beeswax and olive oil) in order to verify whether there is a synergistic antibacterial action between the examined components and to assess the most effective concentration of the examined composites in terms of their antibacterial properties. Due to the fact that the interpretative criteria are not available for the examined type of formulations, the arbitrary criteria were adopted to determine the most effective concentration, which we assumed to be the concentration that inhibited the growth of the highest share of strains. And so, the growth of five out of 11 bacterial strains was inhibited by the SIV4 emulsion, while SIV3 inhibited the growth of three strains, whereas SIV2 and SIV 1 caused very small growth inhibition zone in the case of *S. aureus* type strain ATCC 25923 only. For this reason, the SIV4 was selected as the most effective one, i.e. this concentration was selected as MIC. Interestingly, in the case of *Streptococcus dysgalactiae*, similar growth inhibition was observed in the case of olive oil (16 mm) and SIV4 biocomposite (17 mm). The other biocomposite concentrations did not inhibit the growth of this strain. The results of antibacterial activity determination tests are shown in Fig. 5.

In the second stage of antibacterial activity tests, the SIV4 biocomposite and chitosan were examined against 36 Gram-positive cocci. Seven out of 22 lesions-derived strains (i.e. 31.8%) reacted to the application of beeswax biocomposite-containing emulsions and the growth inhibition zones ranged from 10 to 14 mm (Table S2). Importantly, the growth of the only methicillin resistant *S. aureus* identified in this study was inhibited by the application of beeswax emulsion (Table S2). Growth inhibition was also observed in the case of all-susceptible *S. warneri, S. haemolyticus* (MLSb constitutive type of resistance), lincosamide-resistant *S. simulans, S. epidermidis* (methicillin resistant, MLSb constitutive) and *Arthrobacter woluwensis* (methicillin resistant). The growth of five out of 13 (38.5%) *Staphylococcus* spp. strains isolated from healthy skin was inhibited by the beeswax biocomposite emulsion and the growth inhibition zone was 10–11 mm. When the mean growth inhibition zone of all strains are considered, the values are similar between the strains isolated from skin lesions (mean 3.1 mm, std. dev. 5.21) and typical skin microbiota (mean 3.9 mm, std. dev. 5.2). However, when only these inhibited were considered, the mean value of growth inhibition for Gram-positive cocci isolated from skin lesions was 11.3 mm (std. dev. 1.5), while for skin microbiota it was 10.2 (std. dev. 0.44).

The differences in cell wall composition, cell wall proteins and cell metabolism may be the reason for the observed differences in the bacterial reactions to the applied formulations⁸². Similarly to our study, some researchers reported mild antimicrobial activity of beeswax extracts against Gram-positive and Gram-negative bacteria, as well as against *Candida* yeasts and *Aspergillus* fungi⁸³. Hong⁸⁴ examined antibacterial properties of emulsified Manuka beeswax against *S. aureus*, *S. epidermidis* and *E. coli*, but did not observe growth reduction in agar well diffusion assay, or emulsion-direct contact. The only effective formulation however, did not pass the sensory tests. For this reason, it may become challenging to obtain highly effective antibacterial agent containing

	Contact angle		Surface free energy*			
Sample	Water [°]	Diiodomethane [°]	Polar [mJ/m ²]	Dispersive [mJ/m ²]	Total [mJ/m ²]	
SIV1	85.65	60.45	28.05	4.10	32.15	
SIV2	90.95	39.12	45.13	0.39	45.52	
SIV3	89.65	29.5	50.65	0.23	50.88	
SIV4	90.8	30.6	50.44	0.15	50.59	

Table 4. Wetting angles and the values of free surface energy. *The surface free energy was analysed using the Owens-Wendt method^{51,52}.

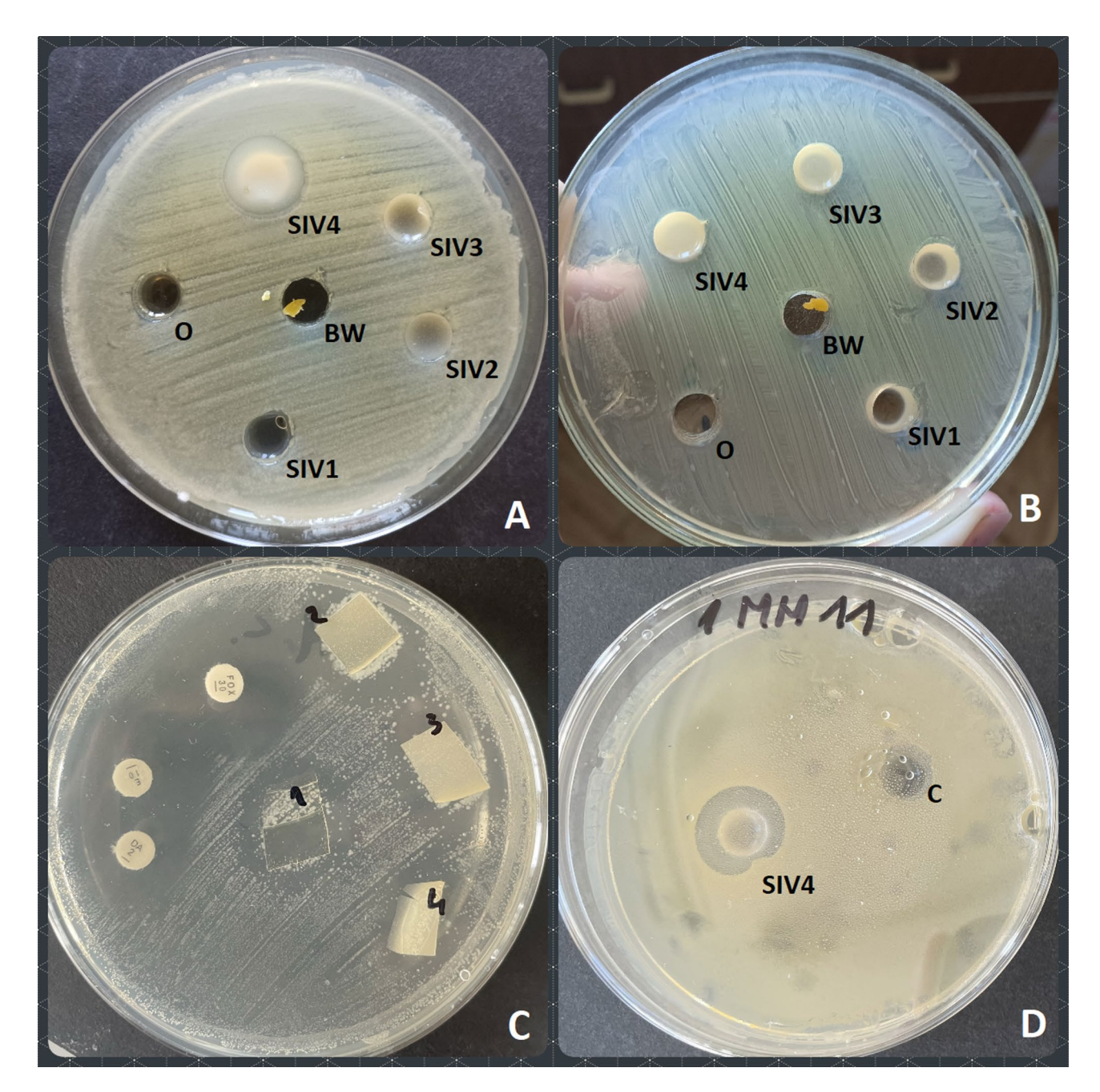


Fig. 5. Reaction of the examined bacterial strains to the biocomposite emulsions. (A) *Escherichia coli* ATCC 25922 tested against SIV1-SIV4 emulsions and olive oil (O) and beeswax (BW) as controls; (B) *Staphylococcus aureus* ATCC 25923 tested against SIV1-SIV4 emulsions and olive oil (O) and beeswax (BW) as controls; (C) *Staphylococcus* spp. tested against SIV1-SIV4 foils and antibiotics (DA, E, FOX discs); (D) *Staphylococcus epidermidis* tested against SIV4 emulsion and control emulsion with no beeswax added (C).

beeswax that would be characterized with high scores of texture and sensory properties. However, what needs to be mentioned here, is that the beeswax-containing biocomposites examined in this study are novel agents, in which the synergism of the three components, i.e. beeswax, olive oil and chitosan, could be the reason for the observed bacterial reactions in the presented experiments, but still the antibacterial activity reported herein cannot be assessed as strong. On the other hand, the mild antibacterial effect that was observed in our study may become useful in production of skincare or cosmetic products that should not damage the natural skin microbiota of their users.

In conclusion, the obtained composites demonstrated selective antimicrobial efficacy against specific pathogens. The methodology for the synthesis of composite materials containing capsules allows for the straightforward incorporation of additional bioactive components into the model system, thereby enhancing the overall antimicrobial efficacy.

Conclusions

The synthesis of capsules comprising beeswax and olive oil, encapsulated in a chitosan matrix, was successfully accomplished. Scanning electron microscope images corroborated the presence of spherical structures in the composites, with diameters ranging from several hundred nanometres to a few micrometres. The degree of both absorption and transparency exhibited by the obtained composites was found to be contingent upon the concentration of the "beeswax/oil" emulsion within the matrix. The incorporation of the capsules resulted in an enhancement of the ultraviolet barrier properties of the resultant films. As the quantity of beeswax present in the samples increases, the thickness of the resulting films also rises; however, this is accompanied by a reduction in their tensile strength and elongation at break. The incorporation of the lowest concentration of the "beeswax/oil" emulsion resulted in an observable increase in the hydrophobicity of the samples, as well as an elevation in the value of the surface free energy. This phenomenon demonstrated a minimal variation with the subsequent elevation in concentration. The resulting composites demonstrated selective antimicrobial efficacy against specific pathogens. The findings suggest that these materials may have potential applications in the cosmetics industry, particularly in products designed to combat specific skin bacteria and protect against UV radiation. Moreover, the materials obtained may also be applicable in the field of food packaging, given their hydrophobic properties. The composites' structural and compositional characteristics render them well-suited for utilisation as model materials, which can be adapted through the incorporation of additional biologically active constituents, contingent upon the intended application.

Data availability

The datasets used and/or analysed during the current study available from the corresponding author on reasonable request.

Received: 9 February 2025; Accepted: 10 September 2025

Published online: 14 October 2025

References

- 1. Zhou, Y., Wang, J., Liang, C. & Zheng, F. Nanotechnology and materials science: Innovations for industry and infrastructure. 375–394 (2024) https://doi.org/10.1007/978-981-97-6184-5_11.
- 2. Guo, J., Khan, M. R., Ahmad, N. & Zhang, W. Enhancing fruit preservation with sodium alginate films incorporating propolis extract and graphene oxide. *Int. J. Biol. Macromol.* **288**, 138778 (2025).
- 3. Salvioni, L. et al. The emerging role of nanotechnology in skincare. Adv. Colloid Interface Sci. 293, 102437 (2021).
- Karnwal, A. et al. Nanotechnology for healthcare: Plant-derived nanoparticles in disease treatment and regenerative medicine. Pharmaceuticals 17, 1711 (2024).
- He, J. et al. Development and characterization of zein co-encapsulated wampee essential oil and propolis extract films for food preservation. Food Control 168, 110855 (2025).
- 6. Janik, M., Hanula, M., Khachatryan, K. & Khachatryan, G. Nano-/microcapsules, liposomes, and micelles in polysaccharide carriers: Applications in food technology. *Appl. Sci.* 13, 11610 (2023).
- 7. Stanisławska, N. et al. Formation and investigation of physicochemical and microbiological properties of biocomposite films containing turmeric extract nano/microcapsules. *Polymers* 15, 919 (2023).
- 8. Janik, M. et al. Preparation and characterisation of acid-base-change-sensitive binary biopolymer films with olive oil and ozonated olive oil nano/microcapsules and added hibiscus extract. *Int. J. Mol. Sci.* 24, 11502 (2023).
- Nowak, N. et al. Preparation of nano/microcapsules of ozonated olive oil in chitosan matrix and analysis of physicochemical and microbiological properties of the obtained films. *Innov. Food Sci. Emerg. Technol.* 82, 103181 (2022).
- 10. Woszczak, L. et al. Physicochemical and functional properties and storage stability of chitosan-starch films containing micellar nano/microstructures with turmeric and hibiscus extracts. *Int. J. Mol. Sci.* 24, 12218 (2023).
- 11. Zhang, W., Xiao, H. & Qian, L. Beeswax-chitosan emulsion coated paper with enhanced water vapor barrier efficiency. *Appl. Surf. Sci.* **300**, 80–85 (2014).
- 12. Sultan, M., Hafez, O. M., Saleh, M. A. & Youssef, A. M. Smart edible coating films based on chitosan and beeswax–pollen grains for the postharvest preservation of Le Conte pear. RSC Adv. 11, 9572–9585 (2021).
- 13. Nandy, A., Lee, E., Mandal, A., Saremi, R. & Sharma, S. Microencapsulation of retinyl palmitate by melt dispersion for cosmetic application. *J. Microencapsul.* 37, 205–219 (2020).
- 14. Pereda, M., Amica, G. & Marcovich, N. E. Development and characterization of edible chitosan/olive oil emulsion films. *Carbohydr. Polym.* 87, 1318–1325 (2012).
- 15. Al-Waili, N. S. Topical application of natural honey, beeswax and olive oil mixture for atopic dermatitis or psoriasis: partially controlled, single-blinded study. *Complement. Ther. Med.* 11, 226–234 (2003).
- 16. Tulloch, A. P. Beeswax: Structure of the esters and their component hydroxy acids and diols. Chem. Phys. Lipids 6, 235-265 (1971).
- 17. O'Neil, M. J. The Merck index: an encyclopedia of chemicals, drugs, and biologicals. (RSC Publishing, 2013).
- 18. Meeting, J. F. E. C. on F. A. & Organization, W. H. Safety evaluation of certain food additives. vol. 65 (World Health Organization, 2006).
- 19. Osae, R. et al. Influence of shea butter, bee wax and cassava starch coatings on enzyme inactivation, antioxidant properties, phenolic compounds and quality retention of tomato (Solanum lycopersicum) fruits. *Appl. Food Res.* 2, 100041 (2022).
- Joseph-Leenose-Helen, J., Noor, N., Mushtaq, M. & Gani, A. Ultrasonics as a tool for development of pine-needle extract loaded bee wax edible packaging for value addition of Himalayan cheese. Ultrason. Sonochem. 82, 105914 (2022).
- Srikantharajah, N., Pakeerathan, K. & Mikunthan, G. Fungicide-free management of papaya anthracnose (Colletotrichum gloeosporioides Penz.) disease using combined bio-rationales and bee wax in organic agriculture. Biol. Life Sci. Forum 4, 16 (2020).
- 22. Gokulakrishnaa, R. K. & Thirunavukkarasu, S. Apitherapy: A valuable gift from honey bee. *J. Entomol. Zool. Stud.* **8**, 2317–2323 (2020).
- 23. Sharma, S. & Kotiyal, A. Bee wax, Aloe vera gel and Carnauba wax impact on chemical shelf life of guava fruits under ambient storage conditions. *Pharma Innov. J.* 11, 3715–3718 (2022).
- 24. Hosseini, S. F., Mousavi, Z. & McClements, D. J. Beeswax: A review on the recent progress in the development of superhydrophobic films/coatings and their applications in fruits preservation. *Food Chem.* **424**, 136404 (2023).
- 25. Badhe, R. V., Adkine, D. & Godse, A. Development of polylactic acid and bovine serum albumin-layered-coated chitosan microneedles using novel bees wax mould. *Turk. J. Pharm. Sci.* 18, 367 (2021).
- 26. Hamid, I. & Stone, N. Bees wax wraps—a novel source of colophonium allergic contact dermatitis. Contact Dermat. 88, 315 (2023).

- 27. Rajabi, S. & Saghafi, M. M. Investigating the antimicrobial effects of amniotic membrane, arnebia euchroma, sesame oil, and bee wax on gram-positive and gram-negative bacteria in second-degree burn wounds. *J. Microb. Biol.* 11, 51–60 (2022).
- Passeri, V. et al. The ancient olive trees (Olea europaea L.) of the Maltese Islands: A rich and unexplored patrimony to enhance oliviculture. Plants 12, 1988 (2023).
- 29. Kiritsakis, A. et al. Olive oil and mediterranean diet: The importance of olive oil constituents, and mainly of its polyphenols, in human health—The redox system—Xenohormesis hypothesis. A Rev. Divers. Neurol. Disord. Pathophysiol. Mol. Mech. Ther. 603–619 (2024) https://doi.org/10.1016/B978-0-323-95735-9.00043-7.
- 30. Dauber, C., Parente, E., Zucca, M. P., Gámbaro, A. & Vieitez, I. Olea europea and by-products: Extraction methods and cosmetic applications. *Cosmetics* 10, 112 (2023).
- 31. Parente, E., Miraballes, M. & Gámbaro, A. Use of completion projective technique to understand consumer's perception upon a novelty cosmetic with olive oil. *J. Sens. Stud.* **38**, e12800 (2023).
- 32. Maestrello, V., Solovyev, P., Bontempo, L., Mannina, L. & Camin, F. Nuclear magnetic resonance spectroscopy in extra virgin olive oil authentication. *Compr. Rev. Food Sci. Food Saf.* 21, 4056–4075 (2022).
- 33. Rodrigues, R., Alves, R. C. & Oliveira, M. B. P. P. Exploring olive pomace for skincare applications: A review. *Cosmetics* 10, 35 (2023)
- 34. Krystyjan, M. et al. Physicochemical, bacteriostatic, and biological properties of starch/chitosan polymer composites modified by graphene oxide designed as new bionanomaterials. *Polymers* 13, 2327 (2021).
- 35. Su, J. et al. Recent functionality developments of carboxymethyl chitosan as an active food packaging film material. *Food Chem.* **463**, 141356 (2025).
- 36. Kumar, A. et al. Chitosan-based composites: development and perspective in food preservation and biomedical applications. *Polymers* 15, 3150 (2023).
- 37. Elsabee, M. Z. & Abdou, E. S. Chitosan based edible films and coatings: A review. Mater. Sci. Eng. C 33, 1819-1841 (2013).
- 38. Zhang, W. et al. Advances in sustainable food packaging applications of chitosan/polyvinyl alcohol blend films. Food Chem. 443, 138506 (2024).
- 39. Fathalian, F., Moghadamzadeh, H., Hemmati, A. & Ghaemi, A. Efficient CO₂ adsorption using chitosan, graphene oxide, and zinc oxide composite. *Sci. Rep.* 14, 1–19 (2024).
- 40. Liu, Z. et al. A review of advancements in chitosan-essential oil composite films: Better and sustainable food preservation with biodegradable packaging. Int. J. Biol. Macromol. 274, 133242 (2024).
- 41. Taheri, M. & Amiri-Farahani, L. Anti-inflammatory and restorative effects of olives in topical application. *Dermatol. Res. Pract.* 2021, 9927976 (2021).
- 42. Skowron, K. et al. Human skin microbiome: impact of intrinsic and extrinsic factors on skin microbiota. *Microorganisms* 9, 543 (2021).
- 43. Byrd, A. L., Belkaid, Y. & Segre, J. A. The human skin microbiome. Nat. Rev. Microbiol. 16, 143-155 (2018).
- 44. Cundell, A. M. Microbial ecology of the human Skin. Microb. Ecol. 76, 113-120 (2018).
- 45. Grice, E. A. & Segre, J. A. The skin microbiome. Nat. Rev. Microbiol. 2011(244), 10 (2011).
- 46. Sanford, J. A. & Gallo, R. L. Functions of the skin microbiota in health and disease. Semin. Immunol. 25, 370-377 (2013).
- 47. Sant'Anna, V., Gurak, P. D., Ferreira Marczak, L. D. & Tessaro, I. C. Tracking bioactive compounds with colour changes in foods a review. *Dye. Pigment.* 98, 601–608 (2013).
- 48. Janik, M., Khachatryan, K., Khachatryan, G., Krystyjan, M. & Oszczęda, Z. Comparison of physicochemical properties of silver and gold nanocomposites based on potato starch in distilled and cold plasma-treated water. *Int. J. Mol. Sci.* 24, 2200 (2023).
- 49. ISO ISO 527-1:2019 Plastics Determination of tensile properties Part 1: General principles. https://www.iso.org/standard/75824.html.
- 50. Krystyjan, M., Khachatryan, G., Ciesielski, W., Buksa, K. & Sikora, M. Preparation and characteristics of mechanical and functional properties of starch/Plantago psyllium seeds mucilage films. *Starch/Staerke* **69**, 1700014 (2017).
- 51. Rudawska, A. & Jacniacka, E. Analysis for determining surface free energy uncertainty by the Owen-Wendt method. *Int. J. Adhes. Adhes.* 29, 451–457 (2009).
- 52. Owens, D. K. & Wendt, R. C. Estimation of the surface free energy of polymers. J. Appl. Polym. Sci. 13, 1741-1747 (1969).
- 53. Kahlmeter, G. et al. European Committee on Antimicrobial Susceptibility Testing (EUCAST) technical notes on antimicrobial susceptibility testing. Clin. Microbiol. Infect. 12, 501–503 (2006).
- 54. Fiebelkorn, K. R., Crawford, S. A., McElmeel, M. L. & Jorgensen, J. H. Practical disk diffusion method for detection of inducible clindamycin resistance in Staphylococcus aureus and coagulase-negative staphylococci. *J. Clin. Microbiol.* 41, 4740–4744 (2003).
- Pryshchepa, O., Pomastowski, P. & Buszewski, B. Silver nanoparticles: Synthesis, investigation techniques, and properties. Adv. Colloid Interface Sci. 284, 102246 (2020).
- 56. Chaparro, L. M. et al. Biowaxes from palm oil as promising candidates for cosmetic matrices and pharmaceuticals for human use. *Materials (Basel)* 16, 4402 (2023).
- Jolayemi, O. S., Tokatli, F. & Ozen, B. UV–Vis spectroscopy for the estimation of variety and chemical parameters of olive oils. J. Food Meas. Charact. 15, 4138–4149 (2021).
- 58. Anil Kumar, K. & Viswanathan, K. Study of UV transmission through a few edible oils and chicken oil. J. Spectrosc. 2013, 540417 (2013)
- 59. Khachatryan, G., Khachatryan, K., Szczepankowska, J., Krzan, M. & Krystyjan, M. Design of carbon nanocomposites based on sodium alginate/chitosan reinforced with graphene oxide and carbon nanotubes. *Polymers* 15, 925 (2023).
- 60. Nowak, N. et al. Synthesis of silver and gold nanoparticles in sodium alginate matrix enriched with graphene oxide and investigation of properties of the obtained thin films. *Appl. Sci.* 11, 3857 (2021).
- Andrade, J. et al. FTIR-ATR determination of protein content to evaluate whey protein concentrate adulteration. LWT 99, 166–172 (2019).
- 62. Sanmugam, A. et al. Synthesis of chitosan based reduced graphene oxide-CeO₂ nanocomposites for drug delivery and antibacterial applications. *J. Mech. Behav. Biomed. Mater.* **145**, 106033 (2023).
- 63. Sathiyabama, M. et al. Green synthesis of chitosan nanoparticles using tea extract and its antimicrobial activity against economically important phytopathogens of rice. Sci. Rep. 14, 1–10 (2024).
- 64. Pang, M. et al. Structure and thermal properties of β-sitosterol-beeswax-sunflower oleogels. *Int. J. Food Sci. Technol.* **55**, 1900–1908 (2020)
- 65. Bhatia, S. et al. Novel applications of black pepper essential oil as an antioxidant agent in sodium caseinate and chitosan based active edible films. *Int. J. Biol. Macromol.* **254**, 128045 (2024).
- 66. Mauricio-Sánchez, R. A., Salazar, R., Luna-Bárcenas, J. G. & Mendoza-Galván, A. FTIR spectroscopy studies on the spontaneous neutralization of chitosan acetate films by moisture conditioning. *Vib. Spectrosc.* **94**, 1–6 (2018).
- 67. Velickova, E., Winkelhausen, E., Kuzmanova, S., Alves, V. D. & Moldão-Martins, M. Impact of chitosan-beeswax edible coatings on the quality of fresh strawberries (Fragaria ananassa cv Camarosa) under commercial storage conditions. *LWT Food Sci. Technol.* 52, 80–92 (2013).
- Tinto, W. F., Elufioye, T. O. & Roach, J. Waxes. In Pharmacognosy fundamentals, applications and strategies 443–455 (2017) https://doi.org/10.1016/B978-0-12-802104-0.00022-6.
- 69. Gaurav, S. Digital color imaging handbook. (CRC press, 2017).

- 70. Oniszczuk, T. et al. Physical assessment, spectroscopic and chemometric analysis of starch-based foils with selected functional additives. *PLoS ONE* **14**, e0212070 (2019).
- 71. Mokrzycki, W. S. & Tatol, M. Colour difference∆ EA survey. Mach. Graph. Vis. 20, 383–411 (2011).
- 72. Khachatryan, G. et al. Synthesis and investigation of physicochemical and biological properties of films containing encapsulated propolis in hyaluronic matrix. *Polymers* 15, 1271 (2023).
- 73. Bhattacharjee, S. DLS and zeta potential What they are and what they are not?. J. Control. Release 235, 337-351 (2016).
- 74. Melro, E. et al. Chitosan films in food applications. Tuning film properties by changing acidic dissolution conditions. *Polymers* 13, 1 (2020).
- 75. Kumar, S., Mitra, A. & Halder, D. Centella asiatica leaf mediated synthesis of silver nanocolloid and its application as filler in gelatin based antimicrobial nanocomposite film. *LWT* 75, 293–300 (2017).
- 76. Grzebieniarz, W. et al. The preparation and characterization of quantum dots in polysaccharide carriers (starch/chitosan) as elements of smart packaging and their impact on the growth of microorganisms in food. *Materials* 14, 7732 (2021).
- 77. Zhong, Y., Song, X. & Li, Y. Antimicrobial, physical and mechanical properties of kudzu starch-chitosan composite films as a function of acid solvent types. *Carbohydr. Polym.* 84, 335–342 (2011).
- 78. Cai, Z., Chen, P., Jin, H. J. & Kim, J. The effect of chitosan content on the crystallinity, thermal stability, and mechanical properties of bacterial cellulose—chitosan composites. *Proc. Inst. Mech Eng. Part C J. Mech. Eng. Sci.* 223, 2225–2230 (2009).
- 79. Eslami, Z., Elkoun, S., Robert, M. & Adjallé, K. A review of the effect of plasticizers on the physical and mechanical properties of alginate-based films. *Molecules* 28, 6637 (2023).
- Giz, A. S. et al. A detailed investigation of the effect of calcium crosslinking and glycerol plasticizing on the physical properties of alginate films. Int. J. Biol. Macromol. 148, 49–55 (2020).
- Gao, C., Pollet, E. & Avérous, L. Properties of glycerol-plasticized alginate films obtained by thermo-mechanical mixing. Food Hvdrocoll. 63, 414–420 (2017).
- 82. Johnston, M., McBride, M., Dahiya, D., Owusu-Apenten, R. & Nigam, P. S. Antibacterial activity of Manuka honey and its components: An overview. *AIMS Microbiol.* 4, 655 (2018).
- 83. Fratini, F., Cilia, G., Turchi, B. & Felicioli, A. Beeswax: A minireview of its antimicrobial activity and its application in medicine. Asian Pac. J. Trop. Med. 9, 839–843 (2016).
- 84. Hong, A. Anti-bacterial properties of emulsified Mānuka beeswax. (2015).

Author contributions

L.W. and K.K.— Conceptualization; L.W., K.K., M.K., A.L.-B., M. Krzan, A.B. and G.K.—methodology; L.W., K.K., M.K., A.L.-B., M. Krzan, A.B. and G.K.—investigation; A.B.—resources; L.W., K.K., M.K., A.L.-B., M. Krzan and G.K.—data curation; L.W., K.K., M.K., A.L.-B. and G.K. writing—original draft preparation; L.W., K.K., M.K., A.L.-B. and G.K.—visualization; K.K. and G.K. – supervision.

Funding

This research was funded by a subsidy from the Ministry of Science and Higher Education for the University of Agriculture in Krakow for 2024 and National Science Center of Poland, grant no. 2022/45/B/ST8/02058.

Declarations

Competing interests

The authors declare no competing interests.

Additional information

Supplementary Information The online version contains supplementary material available at https://doi.org/1 0.1038/s41598-025-19814-w.

Correspondence and requests for materials should be addressed to K.K.

Reprints and permissions information is available at www.nature.com/reprints.

Publisher's note Springer Nature remains neutral with regard to jurisdictional claims in published maps and institutional affiliations.

Open Access This article is licensed under a Creative Commons Attribution-NonCommercial-NoDerivatives 4.0 International License, which permits any non-commercial use, sharing, distribution and reproduction in any medium or format, as long as you give appropriate credit to the original author(s) and the source, provide a link to the Creative Commons licence, and indicate if you modified the licensed material. You do not have permission under this licence to share adapted material derived from this article or parts of it. The images or other third party material in this article are included in the article's Creative Commons licence, unless indicated otherwise in a credit line to the material. If material is not included in the article's Creative Commons licence and your intended use is not permitted by statutory regulation or exceeds the permitted use, you will need to obtain permission directly from the copyright holder. To view a copy of this licence, visit https://creativecommons.org/licenses/by-nc-nd/4.0/.

© The Author(s) 2025